Delicate balance between ferroelectricity and antiferroelectricity in hexagonal $InMnO_3$

F.-T. Huang,[1] X. Wang,[1] Y. S. Oh,[1] K. Kurushima,[2] S. Mori,[3] Y. Horibe,[1] and S.-W. Cheong[1,*]

[1]*Rutgers Center for Emergent Materials and Department of Physics & Astronomy, Rutgers University, Piscataway, New Jersey 08854, USA*

[2]*Toray Research Center, Ohtsu, Shiga 520-8567, Japan*

[3]*Department of Materials Science, Osaka Prefecture University, Sakai, Osaka 599-8531, Japan*

(Received 28 February 2013; revised manuscript received 21 April 2013; published 13 May 2013)

The presence of ferroelectricity in hexagonal $InMnO_3$ has been highly under debate. The results of our comprehensive experiments of low-temperature (T) polarization, transmission electron microscopy, and high-angle annular dark-field scanning TEM on well-controlled $InMnO_3$ reveal that the ground state is ferroelectric with $P6_3cm$ symmetry, but a nonferroelectric $P\bar{3}c1$ state exists at high T and can be quenched to room temperature. We found that the competing ferroelectric and antiferroelectric phases coexist in mesoscopic scales and can be deliberately controlled by varying thermal treatments.

DOI: 10.1103/PhysRevB.87.184109 PACS number(s): 77.80.Dj, 68.37.−d, 77.80.B−

I. INTRODUCTION

Hexagonal manganites (h-$RMnO_3$, R: Y and Ho-Lu) continue to attract a great deal of attention because of its improper ferroelectricity, the presence of topological vortices, and multiferroicity.[1–3] The size mismatch between rare-earth (RE) layers and Mn layers induces a trimerization-type structural phase transition from the high-temperature paraelectric (PE) state ($P6_3/mmc$). In order to achieve favorable close packing, the rigid MnO_5 trigonal bipyramids tilt, which leads to a loss of an inversion symmetry with 2/3 upward- and 1/3 downward-distorted (up-up-down) RE ions along the c axis; this imbalance induces a ferroelectric (FE) state [$P6_3cm$ in Fig. 1(a)].[2] The magnitude of the MnO_5 bipyramid tilting and that of the RE-layer buckling increases naturally with decreasing RE ionic radius due to increasing layer-size mismatch.[4,5] The various physical characteristics of such structural-driven ferroelectricity, including the phase transition temperature (T_c) and the magnitude of ferroelectric polarization are evidently coupled with the size of RE ions.[4–6] $InMnO_3$, where In ions are much smaller than any RE ions in size, does form in a similar hexagonal structure, and thus it is intriguing to find out the possible ferroelectricity in hexagonal $InMnO_3$.

Ferroelectricity in $InMnO_3$ has been highly controversial. $InMnO_3$ was theoretically predicted and experimentally claimed to show weak ferroelectricity with $T_c \sim 500$ K in 2001[7] and 2006,[8] respectively. More recently, despite a fully filled 4d orbital in $InMnO_3$ distinct from $YMnO_3$,[2] Oak *et al.* proposed an alternative intra-atomic $4d_z^2$-$5p_z$ orbital mixing of In and a covalent bonding [$4d_z^2$(In)-$2p_z$(O)] along the c axis, resulting in a ferroelectric ground state.[9] On the other hand, Belik *et al.* reported the absence of spontaneous polarization.[10] In addition, Kumagai *et al.* reported their experimental results of no ferroelectric signals in second-harmonic generation (SHG) and piezoelectric force microscope (PFM) measurements, and concluded a nonpolar structure for $InMnO_3$.[11] Based on density functional theory (DFT) calculations, they also claimed that the ground state is a nonferroelectric state with the space group of $P\bar{3}c1$ even though there exists only a small energy difference between the nonpolar $P\bar{3}c1$ and ferroelectric $P6_3cm$ states. In the nonpolar $P\bar{3}c1$ state, In ions sit equally on 1/3 downward, 1/3 in mirror plane, and 1/3 upward (down-no-up) positions.[11] In frustrated Ising triangular (i.e., hexagonal) antiferromagnets, a PDA state refers to a partially disordered antiferromagnetic state where spins on a honeycomb lattice portion of the hexagonal lattice order antiferromagnetically, and the rest of spins are disordered.[12] Due to the evident analogy, we call the nonpolar $P\bar{3}c1$ a partially undistorted antiferroelectric (PUA) state [Fig. 1(a)]. The preparation of high-quality $InMnO_3$ and the growth of decent-size single crystals turn out to be challenging, which is partially the origin of the controversy. Therefore, it is imperative to find out the correct crystallographic ground state in well-controlled specimens of $InMnO_3$.

In general, x-ray and electron-diffraction methods are the two main powerful and robust techniques to study crystallographic structures. However, the same extinction rules in both FE and PUA states provide difficulties to distinguish them from, for example, x-ray structural refinements, even though slightly different intensity ratios of Bragg peaks exist due to different structural factors. On the other hand, dark-field transmission electron microscopy (DF-TEM) is an ideal and well-known technique to examine domain structures in ferroelectric and nonferroelectric materials because of its high spatial resolution and ability to isolate specific types of domains using a specific diffraction spot.[1,13] In particular, we can examine the existence of inversion symmetry by taking advantage of Friedel's law, where the Friedel-related pairs of Bragg reflections should behave differently in a noncentrosymmetric structure.[13,14] In this paper, we have investigated the domain morphologies of a series of h-$InMnO_3$ specimens prepared in different conditions using DF-TEM as well as high-angle annular dark-field scanning transmission electron microscopy high-angle annular dark-field scaanning TEM (HAADF-STEM) with atom-resolved spatial resolution. We provide conclusive evidence of the presence of the ferroelectric ground state in $InMnO_3$ with characteristic topological vortices. In addition, we demonstrate that the long-range or short-range FE and/or PUA states can be deliberately controlled by varying thermal treatments.

II. EXPERIMENT

Polycrystalline specimens of $InMnO_3$ were prepared by a solid-state reaction method. The mixtures of In_2O_3 (99.999%) and MnO_2 (99.99%) powders with the stoichiometric ratio

were ground together, pelletized, and then heated at 980°C for 200 h in air. A small amount (2–5%) of Bi_2O_3 (99.975%) was added to enhance the grain growth of $InMnO_3$. Using STEM with the energy-dispersive x-ray spectroscopy (STEM-EDX), we estimate that the upper limit for the amount of Bi in $InMnO_3$ grains in all our specimens is 0.4 at. % (see Sec. 1 of the Supplemental Material[15]). Four polycrystalline $InMnO_3$ specimens are discussed in this paper: IMO-*a* was slowly cooled (2°C/h) from 980°C, IMO-*b* was furnace cooled, IMO-*c* was quenched from 950°C, and IMO-*d* was quenched from 650°C to room temperature after being cooled slowly (10°C/h) from 980°C. Polarization vs electric field, $P(E)$, hysteresis loops were measured at $T = 100$ K and a frequency of 13 Hz by using a programmable function generator (DS340), a high-voltage amplifier, and an oscilloscope (TDS1010). In order to compensate leakage contribution, the so-called positive-up-negative-down (PUND) method has been employed.[16] Specimens for TEM studies were prepared by mechanical polishing, followed by Ar ion milling. Domain structures were studied using a JEOL-2010F transmission electron microscope equipped with a 14-bit charge-coupled-device (CCD) array detector. Imaging plates were also used to record dark-field images. All the Miller indices described in this paper are based on $P6_3cm$ structure. HAADF imaging and chemical mapping with an atomic-column resolution were carried out using a JEOL-ARM200F scanning transmission electron microscope equipped with a spherical aberration Cs corrector in conjunction with energy-dispersive x-ray spectroscopy.

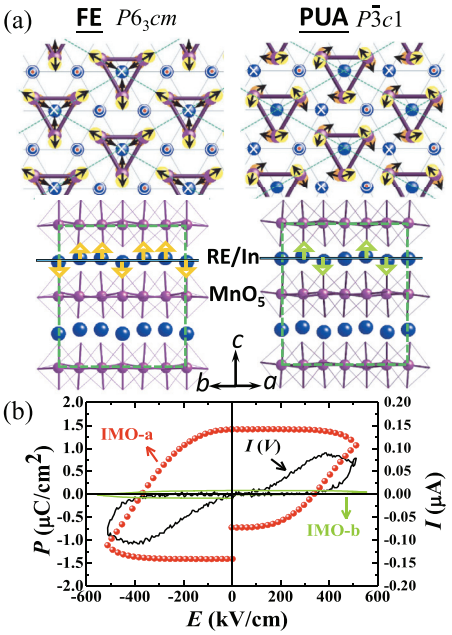

FIG. 1. (Color online) (a) The top and side view of the ferroelectric (FE, $P6_3cm$) and partially undistorted antiferroelectric (PUA, $P\bar{3}c1$) structures of *h*-*R*(In)MnO_3. The navy (large), purple (small), yellow, and orange spheres represent *R*/In, Mn ions, upper, and bottom apical O ions of MnO_5 bipyramids, respectively. The arrows depict the directions of *R*/In and O atomic distortions. The triangles with purple bars correspond to the Mn trimers. The green dashed lines represent the unit cells of the $\sqrt{3} \times \sqrt{3}$ superlattice due to In distortions and Mn trimers. (b) Polarization vs electric field, $P(E)$, hysteresis loops for polycrystalline IMO-*a* (red spheres), IMO-*b* (green solid lines) measured at 100 K and $f = 13$ Hz. The black line depicts the compensated $I(V)$ of IMO-*a* through a PUND measurement. Still, there exists a nonlinear leakage $I(V)$ near the saturation, so the real remnant polarization value may be lower by >25%.

III. RESULTS AND DISCUSSIONS

All four $InMnO_3$ specimens have been confirmed to show a $\sqrt{3} \times \sqrt{3}$ superstructure from the $P6_3/mmc$ paraeletric structure in x-ray diffraction patterns, but their electric properties exhibit surprisingly different behaviors. The $P(E)$ loops of IMO-*a* [Fig. 1(b)] indicate a clear ferroelectric hysteresis character with a remnant polarization (Pr) value of 1.4 $\mu C/cm^2$ while IMO-*b* does not show any hint of Pr. The drastic difference between IMO-*a* and IMO-*b* is consistent with the different domain morphologies revealed in dark-field TEM images. Figure 2(a) is a typical DF-TEM image of IMO-*a* using the $\mathbf{g}^- = (\bar{2}22)$ spot along the [101] direction based on $P6_3cm$, which displays cloverleaf patterns with three Mn-trimerization antiphases (α, β, γ) coupled with opposite polarizations $(+, -)$.[1] These cloverleaf patterns are, in fact, topological defects that are characteristic of the antiphase-ferroelectricity coupled domain configuration in hexagonal manganites.[1] The alternating light and dark contrast results from unequal diffraction intensities associated with antiparallel polarization of the neighboring domains along the [001] direction due to the Friedel pair breaking.[14] Depending on the sign of the vorticity, a topological defect is either a topological vortex or antivortex. These vortices and antivortices tend to be paired, and the typical size of vortex domains in IMO-*a* is about 100–200 nm, which is significantly smaller than that of any *h*-$RMnO_3$, showing vortex domains with the size of a few micrometers.[1,6] The breaking of the inversion symmetry in IMO-*a* is further confirmed in the DF-TEM image obtained using the opposite $\mathbf{g}^+$=$(2\bar{2}\bar{2})$ spot

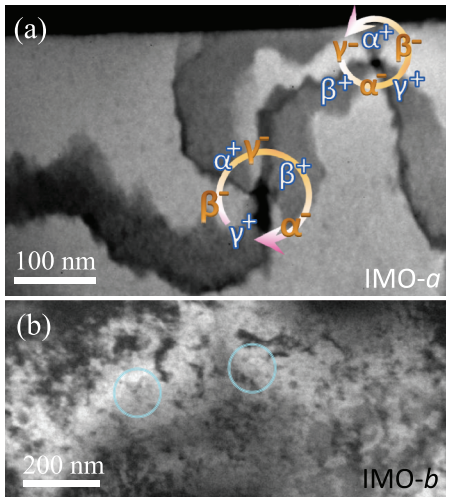

FIG. 2. (Color online) (a) DF-TEM image of slow-cooled IMO-*a*, taken using the $\mathbf{g}^- = (\bar{2}22)$ spot, exhibits topological vortex-antivortex domains, characteristic of the FE $P6_3cm$ state. (b) DF-TEM image of furnace-cooled IMO-*b*, taken using the $\mathbf{g}^+ = (2\bar{2}\bar{2})$ spot, showing numerous nanoscale speckles (sky-blue circle).

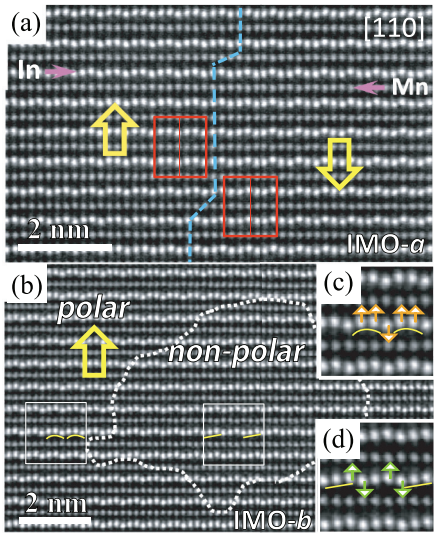

FIG. 3. (Color online) HAADF-STEM image of IMO-*a* (with collected angles of 80–240 mrad and a specimen thickness of 50 nm) exhibits two opposite-polarization domains with a domain wall. The unit cells are schematically shown with red rectangles, and a blue dashed line marks the domain wall with a $2a/3$ displacement (a = 5.8945 Å). Left and right domains show up-up-down and down-down-up In distortions, respectively. (b) HAADF-STEM image of IMO-*b* shows a nanoscale nonpolar domain embedded in the polar matrix. (c, d) Enlarged view of FE up-up-down and nonpolar PUA down-no-up states. The open yellow arrows, orange/green arrows, and yellow lines represent polarization direction, In distortions, and In-distortion schematics, respectively.

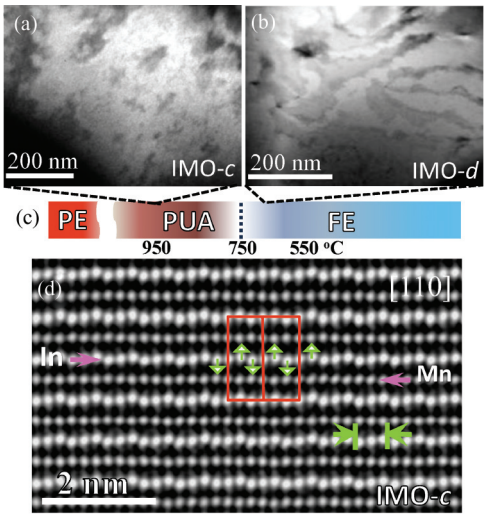

FIG. 4. (Color online) (a, b) DF-TEM images of IMO-*c* (quenched from 950°C) and IMO-*d* (quenched from 650°C). (c) A schematic for the temperature evolution of $InMnO_3$ phases. (d) HAADF-STEM image of IMO-*c* shows a long-range PUA state with down-no-up In distortions. The red rectangles display the unit cells, and green arrows depict atomic In distortions.

[as shown in Fig. S2(a) of the Supplemental Material[15]]. The contrasts in Fig. S2(a) are reversed from those in Fig. 2(a), which unambiguously demonstrates the Friedel pair breaking due to the noncentrosymmetrical structure of $InMnO_3$. On the other hand, the DF-TEM image of IMO-*b* in Fig. 2(b) shows diffusive contrasts and many nanometer-sized dark speckles indicated by sky-blue circles. It is plausible that the speckle-type pattern turns into vortex domains when a specimen is cooled slowly from the synthesis temperature. Note that the breaking of the Friedel pairs does not take place for those speckles, indicating that those speckles contribute to the $\sqrt{3} \times \sqrt{3}$ superlattice peaks but are not associated with the inversion symmetry breaking (see Sec. 3 of the Supplemental Material[15]).

In order to probe directly the atomic configuration of the ferroelectric state, we obtained HAADF-STEM images of IMO-*a*, which exhibits nice vortex domains in DF-TEM images. Figure 3(a) shows a typical HAADF-STEM image (8 nm × 5 nm) of IMO-*a*, including two regions with opposite polarization orientations (hollow arrows) with an type I antiphase domain boundary (APB-I) (blue dashed line).[1] It is a [110] projection view with the sequence of In (top)-Mn-In-· · ·-In (bottom) layers and shows bright spots corresponding to heavy In ions and weak ones corresponding to light Mn ions. Note that the assignment of In and Mn ions has been verified by element-specific images using a STEM-EDX technique (see Sec. 1 of the Supplemental Material[15]). The In ions display clearly the off-center shift with "up-up-down" (left) or "down-down-up" (right) distortions, but the Mn ions are well aligned without the indication of any off-center shift. The combination of the noncentrosymmetric feature in DF-TEM images, the observation of atomic-scale up-up-down or down-down-up In distortions in the HAADF-STEM images, and the existence of Pr in $P(E)$ loops indicate unambiguously the presence of ferroelectricity in slowly cooled IMO-*a*. On the other hand, a HAADF-STEM image on furnace-cooled IMO-*b* [Fig. 3(b)] exhibits a few-nanometer-scale region with a nonpolar "down-no-up" In configuration (i.e., PUA, green arrows) embedded in the polar up-up-down matrix (i.e., FE, orange arrows). Figures 3(c) and 3(d) display two enlarged FE and PUA regions. The existence of such nanoscale PUA islands, which appear to correspond to speckles in DF-TEM images [Fig. 2(b)], is certainly different from the behavior of the thin domain walls with down-no-up distortions, which were first proposed as a possible configuration for the ferroelectric-trimerization domain walls in hexagonal $YMnO_3$,[1] studied theoretically[17] and also observed experimentally.[18] We emphasize that in IMO-*b*, the PUA islands are very common, but the dominant phase is still the FE matrix.

In order to clarify the origin of the PUA islands in IMO-*b*, we performed DF-TEM and HAADF-STEM experiments on specimens from two different annealing temperatures [950°C (IMO-*c*) and 650°C (IMO-*d*)]. Figure 4(a) shows a DF-TEM image of IMO-*c*, which exhibits no hint of the vortex-type domains, and a HAADF-STEM image [Fig. 4(d)], in fact, demonstrates a long-range PUA state—i.e., down-no-up In distortions are everywhere in the image. On the other hand, IMO-*d* exhibits small vortex-antivortex domains (50–200 nm in size) with highly curved boundaries as shown in Fig. 4(b), which indicates the presence of a ferroelectric state. Furthermore, when a specimen was quenched from 750°C, its behavior was in between those of IMO-*c* and IMO-*d*—i.e., a mixture of very fine vortex-antivortex domains and PUA islands. A fast-quenching process tends to induce

large leakage, so reliable $P(E)$ data on IMO-*c* and IMO-*d* were not obtained. However, the domain features clearly indicate a PUA state in IMO-*c* and a ferroelectric state in IMO-*d*. These results suggest strongly that the PUA is a stable state near 950°C, the high-temperature PUA can be quenched to room temperature, the transition from the high-temperature PUA to the low-temperature FE is very sluggish, and the ground state is FE.[10,11] The evolution of the structural phase in $InMnO_3$ is schematically illustrated in Fig. 4(c). Note that $P6_3cm$ and $P\bar{3}c1$ are subgroups of $P6_3/mmc$, but $P6_3cm$ and $P\bar{3}c1$ have no subgroup relationship to each other, so it is expected that the transition between $P6_3cm$ and $P\bar{3}c1$ is first-order type.

In summary, from comprehensive characterization of well-controlled specimens, we have clarified the long-standing dispute of the ferroelectric state of $InMnO_3$ and identified that the ground state is a ferroelectric state with $P6_3cm$ symmetry. In addition, the ferroelectric ground state accompanies topological vortex domains, similar to what was observed in *h*-$RMnO_3$. On the other hand, we have demonstrated the existence of an intermediate centrosymmetric structure with $P\bar{3}c1$ symmetry. Furthermore, we found that the transition from the intermediate centrosymmetric to the ferroelectric ground states is unusually sluggish. Our findings reveal the rich nature of structure-driven improper ferroelectricity.

ACKNOWLEDGMENTS

The work at Rutgers was supported by the NSF under Grant No. DMR-1104484 and the National Science Council of Taiwan under Project No. 101-2917-I-564-077.

*sangc@physics.rutgers.edu

[1] T. Choi, Y. Horibe, H. T. Yi, Y. J. Choi, Weida Wu, and S.-W. Cheong, Nat. Mat. **9**, 423 (2010).
[2] B. B. V. Aken, T. T. M. Palstra, A. Filippetti, and N. A. Spaldin, Nat. Mater. **3**, 164 (2004).
[3] C. J. Fennie and K. M. Rabe, Phys. Rev. B **72**, 100103 (2005).
[4] T. Katsufuji, M. Masaki, A. Machida, M. Moritomo, K. Kato, E. Nishibori, M. Takata, M. Sakata, K. Ohoyama, K. Kitazawa, and H. Takagi, Phys. Rev. B **66**, 134434 (2002).
[5] B. B. VanAken and T. T. M. Palstra, Phys. Rev. B **69**, 134113 (2004).
[6] S. C. Chae, N. Lee, Y. Horibe, M. Tanimura, S. Mori, B. Gao, S. Carr, and S.-W. Cheong, Phys. Rev. Lett **108**, 167603 (2012).
[7] S. C. Abrahams, Acta. Cryst. **B57**, 485 (2001).
[8] C. R. Serrao, S. B. Krupanidhi, J. Bhattacharjee, U. V. Waghmare, A. K. Kundu, and C. N. R. Raoa, J. Appl. Phys. **100**, 076104 (2006).
[9] M.-A. Oak, J.-H. Lee, H. M. Jang, J. S. Goh, H. J. Choi, and J. F. Scott, Phys. Rev. Lett **106**, 047601 (2011).
[10] A. A. Belik, S. Kamba, M. Savinov, D. Nuzhnyy, M. Tachibana, E. Takayama-Muromachi, and V. Goian, Phys. Rev. B **79**, 054411 (2009).
[11] Yu Kumagai, A. A. Belik, M. Lilienblum, N. Leo, M. Fiebig, and N. A. Spaldin, Phys. Rev. B **85**, 174422 (2012).
[12] M. Mekata, J. Phys. Soc. Jpn. **42**, 76 (1977).
[13] M. Tanaka and G. Honjo, J. Phys. Soc. Jpn. **19**, 954 (1964).
[14] R. Gevers, H. Blank, and S. Amelinckx, Phys. Stat. Sol. **13**, 449 (1966).
[15] See Supplemental Material at http://link.aps.org/supplemental/10.1103/PhysRevB.87.184109 for the details of the STEM-EDX result, the evidence of non-centrosymmetric ferrolectric state and centrosymmetric antiferroelectric state in $InMnO_3$.
[16] J. F. Scott, C. A. Araujo, H. B. Meadows, L. D. McMillan, and A. Shawabkeh, J. Appl. Phys. **66**, 1444 (1989).
[17] Y. Kumagai and N. A. Spaldin, Nat. Commun. **4**, 1540 (2013).
[18] Q. H. Zhang, L. J. Wang, X. K. Wei, R. C. Yu, L. Gu, A. Hirata, M. W. Chen, C. Q. Jin, Y. Yao, Y. G. Wang, and X. F. Duan, Phys. Rev. B **85**, 020102 (2012).